Seismic Hazard Assessment for Proposed Stimulation Activities at the West Newton Site

June 2024

Report Commissioned by Rathlin Energy Ltd

Report Internal ID: OLG.RA-WN-SHA

Authors:
Dr. James Verdon, Lead Geophysicist, Outer Limits Geophysics LLP

Summary

- Rathlin Energy Ltd. plans to conduct a reservoir stimulation operation in the West Newton WNA-2 well. This operation involves the injection of a total of approximately 60 m^3 of fluid into the well. In this study we assess the potential induced seismicity hazard that could be associated with this type of activity.
- This type of small-scale conventional reservoir stimulation has no past record of causing induced seismicity. Induced seismicity has only been associated with large scale, high volume hydraulic fracturing of shale gas formations, which uses injection volumes that are orders of magnitude higher than the operation under consideration here.
- The West Newton site is located in an area with relatively low rates of natural seismicity. Various reservoir stimulation activities have taken place in the region, including at the Beckingham, Corringham, Gainsborough, Malton and Kirby Misperton fields. No induced seismicity was associated with any of these past activities. Stimulation at the nearby Wressle field in 2021 was monitored by a dedicated microseismic array, but this did not detect any events.
- Rathlin have mapped faults in the Kirkham Abbey Formation using 3D reflection seismic surveys. The nearest mapped fault is approximately 1 km from the well. This is much further than the maximum possible perturbation is expected to reach (the expected fracture length is less than 20 m).
- We have conducted a geomechanical stability assessment on the mapped faults. The stress conditions on the faults are moderate. The Kirkham Abbey Formation is over-pressured, but the critical pore pressures on the faults are lower than those experienced for the Bowland Shale at Preston New Road.
- We have examined the magnitude thresholds at which unacceptable nuisance impacts might be experienced by nearby populations. We define a magnitude of M 2.5 as a threshold of tolerability at which the nuisance associated with the resulting vibrations would become unacceptable.
- We conduct a probabilistic seismic hazard assessment using the seismogenic index method. We define a logic tree of seismogenic index values based on our geomechanical assessment, combined with observations from similar past activities in the region. This assessment finds that the most likely largest event size is a magnitude of M -2.0. There is a 95 % likelihood that the largest event is less than M 0.0, and a 99 % likelihood that the largest event is less than M 0.8.
- The 99 % exceedance event, M 0.8, would not be felt at the surface. The most likely largest event (M -2.0) would not be detectable even with a dedicated local monitoring array. As such, we conclude that the proposed activities pose a very low risk with respect to induced seismicity.
- The installation of a local seismicity monitoring array is not warranted, given the very low levels of risk posed by the proposed operation, and the fact that the planned injection volume is so low that the injection process itself will be very short. This would leave no window for reactive decision-making in response to recorded induced seismicity, rendering any monitoring data of very little operational use.

Copyright Statement

All material is copyright. It may be produced in whole or in part subject to the inclusion of an acknowledgement of the source, but should not be included in any commercial usage or sale. Reproduction for purposes other than those indicated above requires the written permission of the authors.

1. Introduction

Rathlin Energy Ltd. plans to conduct a reservoir stimulation operation in the West Newton WNA-2 well. This operation involves the injection of a total of approximately 60 m^3 of fluid into the well, combined with proppant, which will create permeable pathways linking the reservoir to the well. This type of activity is also sometimes referred to as a proppant squeeze. The Rathlin well plans detail the operational parameters, and includes models of the expect fracture propagation, which are expected to extend less than 20 m from the well. The operation will be conducted into the Permian-age Kirkham Abbey Formation, which forms part of the Zechstein Group of evaporites, carbonates and mudstones.

In this report we conduct an assessment of the induced seismicity hazard posed by the proposed operations. In Chapter 2 we briefly review the phenomenon of hydraulic fracturing-induced seismicity (HF-IS), and in particular how levels of seismicity vary between and within basins, and on the specific nature of the stimulation operation. In Chapter 3 we examine the seismological setting at the site, and past seismicity in the region. We compare these observations with past oilfield operations, finding no occurrence of detected seismicity associated with previous reservoir stimulation activities in the region that were similar to that proposed by Rathlin for the WNA-2 well. In Chapter 4 we examine the geomechanical conditions at the site, and in particular the in situ stress conditions relative to the orientations of faults identified in Rathlin's geophysical surveys of the site, and whether they might be prone to reactivation. In Chapter 5 we evaluate the possible impacts to nearby populations from the shaking that could be generated by low to moderate magnitude induced events. In doing so, we estimate the magnitudes at which the nuisance and/or damage could reach levels that would not be considered acceptable by the local population. In Chapter 6 we perform a seismic hazard assessment for the proposed activity, based on widely accepted links between injection volumes and seismicity rates, in order to quantify the likelihood of felt or damaging events being generated. Finally, in Chapter 7 we provide our conclusions.

Before commencing this analysis, it is necessary to clarify some terminology, since certain terms that are widely used among petroleum engineers are often misinterpreted by non-experts, leading to confusion among the public. Hydraulic fracturing, or hydraulic stimulation, describes a technology used to enhance production from hydrocarbon wells. Fluids are injected at pressure into the formation to generate fractures. Once injection stops, proppant that is mixed with the injected fluid remains in the newly created fractures, producing a permeable pathway linking reservoir rocks to the well, along which hydrocarbons can flow. A single hydraulic fracturing stage typically takes a few hours to complete, although for wells with multiple stages the overall process can therefore take several days. Once the stimulation process is complete, hydrocarbons are allowed to flow from the well over years and even decades, much like any other unstimulated well.

Hydraulic fracturing has been used to stimulate oil and gas reservoirs since the late 1940s (Hubbert and Willis, 1957; Montgomery and Smith, 2010). Prior to the invention of this technology, reservoir stimulation was often achieved using explosive charges (Montgomery and Smith, 2010). Rubinstein and Babaie Mahani (2015) estimate that hydraulic fracturing has been used to stimulate over one million wells in North America alone. Onshore in the UK, over 200 wells have received hydraulic stimulation of some kind.

While the technology of hydraulic fracturing is well established, the nature and scale of the technique has varied significantly both with time, and with the type of reservoir being targeted. It is important to distinguish between a reservoir stimulation or proppant squeeze in a conventional reservoir, hydraulic fracturing in tight sandstone reservoirs, and hydraulic fracturing in shale reservoirs. To date, induced seismicity has only been associated with large-scale hydraulic fracturing of very low permeability shale formations. Such operations typically entail the injection of thousands of m^3 of fluid.

Reservoir stimulation is commonly used in conventional reservoirs. The drilling process itself may create a zone of low permeability around a well, that limits flow from the reservoir. Reservoir stimulation creates a network of fractures that are a few tens of meters long, extending through this low permeability zone and providing a connection with the reservoir. These activities typically use less than 200 m^3 of injected fluid per stage.

As such, "hydraulic fracturing" has become a catch-all term that can be used to describe oilfield activities that take place across a wide range of scales, from very minor reservoir stimulation activities in conventional wells to very large-scale shale gas stimulation projects. In this report we use the terms "hydraulic fracturing" or "stimulation" to refer generically to all of the above technologies where fluids are injected into a reservoir in order to generate fractures that enhance production. Where it is necessary to differentiate between these different types and scales of technique, we do so accordingly.

In the Infrastructure Act 2015, hydraulic fracturing is defined as (emphasis added):

> *hydraulic fracturing of* ***shale or strata encased in shale*** *which […] involves, or is expected to involve, the injection of*
>
> > *(i)* ***more than 1,000 cubic metres of fluid*** *at each stage, or expected stage, of the hydraulic fracturing, or*
> >
> > *(ii)* ***more than 10,000 cubic metres of fluid in total****.*

It can be seen that this definition is specifically intended to apply to large-scale, high volume hydraulic fracturing of shale gas formations. The reservoir stimulation activities proposed here are not into shale (or strata encased in shale), and the volumes involved are much less than 1,000 m^3. Hence, the definitions of hydraulic fracturing as per the Infrastructure Act 2015 do not apply here.

2. Review of Hydraulic-Fracturing Induced Seismicity

In this chapter we review the phenomenon of induced seismicity associated with hydraulic fracturing and other well completion activities. Of particular importance is to understand the physical mechanisms that drive the occurrence of induced seismicity, and to consider how geological conditions and operational factors can serve to increase or mitigate the likelihood of experiencing induced seismicity.

2.1. Hydraulic Fracturing and Induced Seismicity

The term "induced seismicity" refers to earthquakes that are caused by human activities in the subsurface. A distinction is commonly made between "driven" and "triggered" seismicity, where "driven" refers to events whose total slip is comparable to the scale of deformation caused by the activity, while "triggered" refers to events where the earthquake slip is much larger than the scale of deformation, with a smaller human-induced perturbation triggering the release of stresses that have accumulated over geologic time.

The energy released by triggered earthquakes has been stored in the crust over geological time from tectonic processes. Where subsurface fluid injection affects the stress or pore-pressure conditions on a fault such that it is pushed towards slip, this may generate a triggered earthquake that releases the stored tectonic strain energy. With reference to the above terminology, sequences of HF-IS of sufficient magnitude to be of concern are generally triggered events. However, in this report we use the term "induced" in a generic manner to refer to both driven and triggered events, as is common practice.

Hydraulic fracturing is used to enhance the flow characteristics of low permeability reservoirs. It has been widely used since its invention in 1947 (Hubbert and Willis, 1957). By design, hydraulic fracturing creates fractures in the subsurface that are then filled with proppant. The hydraulic fracturing process commonly generates low magnitude ($M < 0$) *microseismic* events. These can be monitored with downhole geophone arrays, and this microseismic data is used to image the fracture dimensions and orientations in the subsurface (e.g., Maxwell et al., 2010). Events of this nature are far too small to be felt at the surface. This operationally-induced microseismicity should not be confused with induced seismicity, where injection causes slip on a pre-existing tectonically stressed fault, creating larger events that might be felt at the surface.

The first widely reported case of hydraulic fracturing induced seismicity occurred in the UK at the Preese Hall well near Blackpool in 2011 (Clarke et al., 2014), which was targeting the Bowland Shale Formation. Hydraulic fracturing induced seismicity was also occurring in the West Canadian Sedimentary Basin (WCSB) in the Horn River area between 2009 – 2011 (BCOGC, 2012; Farahbod et al., 2015), although these events were not widely reported at the time. Since then, awareness of the potential for hydraulic fracturing induced seismicity has increased substantially. Examples have been documented from Ohio, Oklahoma, Arkansas and Texas in the USA (e.g., Friberg et al., 2014; Skoumal et al., 2015, 2018, 2020; Yoon et al., 2017); from the Duvernay and Montney formations in the WCSB; from the Sichuan Basin in southern China (e.g., Lei et al., 2017; 2019); and from the Bowland Shale in the UK (Clarke et al., 2019; Kettlety et al., 2021). The WCSB is probably the most extensively studied basin for HF-IS in the world.

Magnitudes of events induced by hydraulic fracturing have typically been moderate, with $M < 4$ (e.g., Clarke et al., 2014; Farahbod et al., 2015; Yoon et al., 2017; Skoumal et al., 2018, 2020). However, in the

WCSB the largest magnitudes have ranged between $4 < M < 5$ (e.g., Babaie Mahani et al., 2017; Schultz et al., 2017; Babaie Mahani et al., 2019), and in the Sichuan Basin the largest magnitudes have ranged between $5 < M < 6$ (e.g., Lei et al., 2019).

2.2. Mechanisms for Induced Seismicity

The mechanisms by which hydraulic fracturing induced seismicity occur are typically understood by reference to the Mohr Coulomb failure criteria, whereby *in situ* stress conditions are resolved into normal (σ_n) and shear (τ) stresses acting on a fault, and slip will occur if

$$\tau > \mu(\sigma_n - P) + C, \tag{2.1}$$

where P is the pore pressure, μ is the friction coefficient and C is the cohesion. Equation 2.1 can be re-written in terms of the Coulomb Failure Stress, *CFS*:

$$CFS = \tau - \mu(\sigma_n - P), \tag{2.2}$$

where $\sigma_n - P$ is the effective normal stress σ'_n. A positive change in *CFS* implies that the stress conditions are moving towards the failure threshold, increasing the likelihood of induced seismicity.

Equation 2.2 shows that failure can be reached in a number of ways: by increasing the shear stress; by decreasing the normal stress; or by increasing the pore pressure. The primary driving mechanism for HF-IS is the increase in pore pressure, which reduces the effective normal stress (Terzaghi, 1943), moving faults towards the Mohr-Coulomb failure envelope and allowing slip. However, other mechanisms such as stress transfer through poroelastic expansion of the rock frame (e.g., Deng et al., 2016), aseismic slip on pre-existing faults (e.g., Eyre et al., 2019), and stress transfer from tensile fracture opening (e.g., Kettlety et al., 2020) have also been proposed (Figure 2.1).

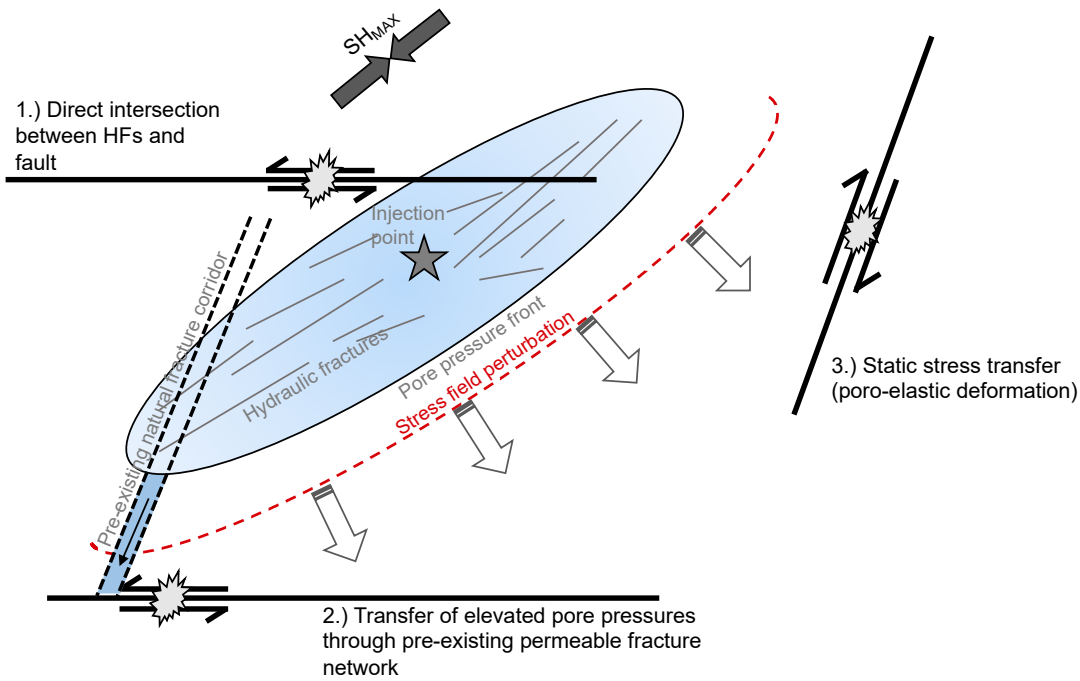

Figure 2.1: Illustration of the mechanisms by which seismicity is induced (or triggered) during hydraulic fracturing.

HF-IS therefore requires certain necessary conditions: (i) injection must create a perturbation in pore pressure or stress conditions; (ii) a pre-existing tectonic fault must be present; (iii) the fault must be close to its critical stress condition (the point in Mohr-Coulomb space at which slip will occur); (iv) the fault must have sufficient surface area such that an event of appreciable magnitude can occur on it; (v) there must be a plausible mechanism by which the pore pressure or stress perturbation can reach the fault and increase the CFS; and (vi) the frictional properties of the fault must be such that the slip is released rapidly as a seismic event (as opposed to slow, aseismic slip).

The presence or absence of these conditions will therefore determine the susceptibility of an operation, region or play to induced seismicity. The presence or absence of the necessary conditions described above will also determine the distances from the well at which induced seismicity might be expected to occur.

2.3. Variability in Hydraulic Fracturing-Induced Seismicity Response

The susceptibility of different formations and plays to HF-IS is observed to vary significantly (Verdon and Rodriguez-Pradilla, 2023). Some plays, such as the Barnett, Bakken and Marcellus in the USA have seen extensive hydraulic fracturing with little or no induced seismicity while others such as the Duvernay and Montney formations in the WCSB, and the Sichuan Basin in China, have produced very high levels of HF-IS.

Verdon and Rodriguez-Pradilla (2023) evaluated the levels of HF-IS in shale plays across North America, finding that rates of seismicity are correlated with the pore pressure and in situ stress conditions, with seismicity being promoted by elevated pore pressures and higher compressive stresses. This behaviour is consistent with the theoretical considerations presented in Equations 2.1 and 2.2. Other geomechanical conditions also have important impacts on the resulting levels of induced seismicity.

The susceptibility to induced seismicity can vary between different geological formations within the same basin. For example, in the Appalachian Basin HF-IS is prevalent during hydraulic fracturing of the Ordovician-age Utica formation, where this unit is in proximity to the Precambrian Basement. In contrast, induced seismicity is very rare from stimulation of the Devonian Marcellus Formation (Skoumal et al., 2018; Verdon and Rodriguez-Pradilla, 2023). The Marcellus is more than 1 km shallower than the Utica (Figure 2.2). Skoumal et al. (2018) argue that the Salina evaporites provide a hydraulic and mechanical barrier that prevents pore pressure and stress perturbations created by stimulation of the Marcellus from propagating downwards into the underlying basement, where pre-existing faults will be more common, and stress gradients may be higher.

Similarly, in the WCSB hydraulic fracturing of the Duvernay and Horn River Shales (Devonian age), and in the Montney Shale (Triassic age) has generated significant levels of HF-IS. However, extensive stimulation of overlying Cretaceous-age tight sandstones such as the Cardium and Mannville Formations has not produced any recorded cases of induced seismicity. Again, depths to basement rocks and in situ

stress conditions are likely to be a key control on the different observed behaviours (Verdon and Bommer, 2021a).

The situation in the WCSB has clear relevance for the West Newton site. In the WCSB there are large differences in the levels of HF-IS that are produced by stimulation of shallower conventional reservoirs versus stimulation of deep underlying shale formations using high injection volumes. These differences are recognised in the regulations that are imposed by the regulator to manage induced seismicity, with more stringent regulations being applied to hydraulic fracturing in deep shales versus smaller-scale operations in shallow, conventional formations (AER 2019a;b).

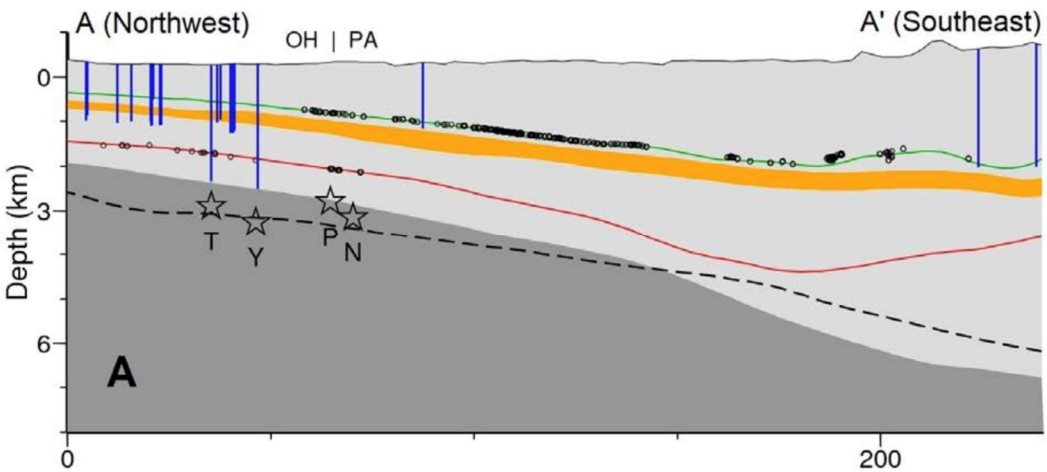

Figure 2.2: Cross-section showing relationship between cases of induced seismicity (stars) and subsurface operations in the Appalachian Basin (Ohio and Pennsylvania), from Skoumal et al. (2018). The blue vertical lines show wastewater disposal wells, and the black dots show hydraulic fracturing in the Marcellus Shale (green line) and Utica Shale (red line). The orange shading shows the Salina evaporites, which present a geomechanical and hydraulic barrier between the two formations. The Pre-Cambrian basement is shaded dark grey. Cases of induced seismicity occur when fluid injection occurs in basal formations, and is more prevalent during stimulation of the deeper Utica shale, even though far more stimulation has taken place in the shallower Marcellus.

The productivity of HF-IS can be described using the seismogenic index, Σ (Shapiro et al., 2010). This parameter is based on the observation that the number of induced earthquakes larger than a specified magnitude increases in proportion to the injected fluid volume (Shapiro and Dinske, 2009). As a result, the Gutenberg and Richter (1944) (GR hereafter) earthquake recurrence relationship, which describes the number, N, of earthquakes larger than magnitude M:

$$\log(N) = a - bM, \tag{2.3}$$

where a and b are constants to be determined empirically, can be reformulated as:

$$\log(N) = \Sigma + \log(V) - bM \tag{2.4}$$

where V is the cumulative injected volume. Hence the seismogenic index describes the ratio of the number of events, $N_t(M)$, larger than magnitude M at time t, to the injected volume at this time, V_t:

$$\Sigma = \log\left(\frac{N_t(M)}{V_t}\right) + bM \tag{2.5}$$

Therefore, the seismogenic index is effectively a measure of how seismically sensitive the rock is to fluid injections at any particular location.

Dinske and Shapiro (2013) show that Σ typically remains constant during injection at a given site. Moreover, Dinske and Shapiro (2013) show extreme variability in Σ between sites, with a difference of over 10 orders of magnitude in the induced seismic response for different injection projects (Figure 2.3). The hydraulic fracturing cases considered by Dinske and Shapiro (2013) sit towards the lower end of their range of Σ values. However, recent cases of hydraulic fracturing induced seismicity in the Horn River Basin, in the Duvernay, and in the Bowland Shale, UK, have produced values of $-2.5 < \Sigma < -0.5$ (e.g., Verdon and Budge, 2018; Schultz et al., 2018; Clarke et al., 2019), towards the higher end of the range identified by Dinske and Shapiro (2013). This variability highlights how the geomechanical conditions at different sites have a significant influence on the occurrence of induced seismicity.

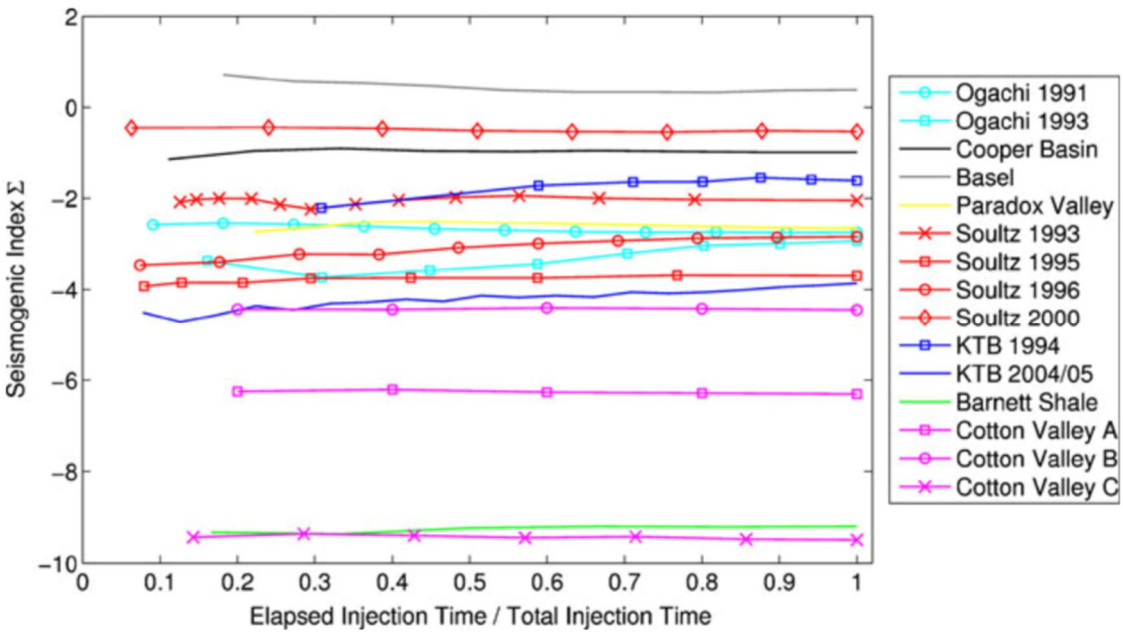

Figure 2.3: Seismogenic index from a selection of injection projects (including waste disposal, geothermal projects, and hydraulic fracturing), from Dinske and Shapiro (2013). The productivity of induced seismicity generation varies by 10 orders of magnitude between these projects.

This variability has been explained in various ways, most of which refer back to the necessary conditions described above. Pre-existing faults of sufficient dimensions must be present, in sufficient proximity to the injection site, these faults must be near to their critical stress conditions, and they must release slip rapidly as seismic events, rather than aseismic slow slip. Therefore, induced seismicity will be more likely in rocks that have a higher abundance of faulting, and in rocks that have significant overpressure (since this will reduce the effective normal stress) or stress anisotropy (since this will increase the shear stress). The proximity of injection to the underlying crystalline basement has often been invoked as a key factor for induced seismicity (e.g., Verdon, 2014; Skoumal et al., 2018; Hincks et al., 2018; Pawley et al., 2018), since the basement will typically be more faulted and, being stiffer (i.e., higher shear modulus), will bear higher stresses (e.g., Vilarrasa and Carrera, 2015), and therefore will host more, and larger, seismic events.

For most of its history, therefore, hydraulic fracturing took place in conventional and tight sandstone and carbonate reservoirs, and was not associated with induced seismicity, leading the National Research Council to state that hydraulic fracturing "*does not pose a high risk for inducing felt seismic events*" (NRC, 2013). To date, we are not aware of any cases of induced seismicity associated with hydraulic fracturing in conventional reservoirs or in tight sandstone or carbonate formations. In contrast, the recent increase in cases of HF-IS has been associated with the increase in the use of large-scale hydraulic fracturing in deep shale formations. Many shale formations have not generated any induced seismicity. Importantly, where seismicity has been associated with hydraulic fracturing, it has only occurred when shale plays have been the target of high volume hydraulic fracturing.

A combination of explanations may be considered to account for the difference in behaviour between conventional reservoirs and some shale plays. The injection volumes used for stimulation of shale gas formations are typically substantially larger than those used in conventional formations – rates of induced seismicity are observed to correlate with injection volume (e.g., Shapiro et al., 2010; van der Elst et al., 2016; Hallo et al., 2014). The permeabilities of conventional formations are orders of magnitude larger than shale formations, which means that elevated pressures during stimulation will quickly dissipate, whereas in lower-permeability shales elevated pore pressures may persist for a longer period of time unless flowback is conducted. In many basins, shale gas plays are found at greater depths, near to basement rocks – as described above, proximity to basement rocks is often an important factor controlling the susceptibility to induced seismicity.

The relative importance of these factors has not received extensive investigation. Nevertheless, it is clear that the levels of induced seismicity produced by hydraulic stimulation of some shale formations are very different to those generated by stimulation of conventional reservoirs. Therefore, assessments of seismic hazard derived from observations and/or modelling of shale formations cannot be applied to conventional reservoirs.

These considerations will be included in the evaluation of induced seismicity hazard presented in Chapter 6.

3. Seismicity and Stimulation Activities in the Vicinity of West Newton

In this chapter we examine the regional seismic context for the proposed operations. We begin by examining the occurrence of earthquakes within a study region comprising a 100 × 100 km square centred on the West Newton site, including a consideration of the detection thresholds provided by the British Geological Survey (BGS) national seismic network, the depths at which events have occurred, and their relationship to industrial activities in the region.

3.1. Seismicity in the West Newton Study Region

Figure 3.1 shows all earthquakes available from the BGS national catalogue, from 1970 to the present. Broadly speaking, levels of seismicity in England decrease from the NW to the SE, with the study area lying in a region of relatively low baseline levels of seismicity. Figure 3.2 shows all earthquakes within the 100 × 100 km square centred on the West Newton site. In total, four events with M ≥ 3.0 have occurred in the study region over a duration of 50 years, indicating that earthquakes in this area are generally small and uncommon.

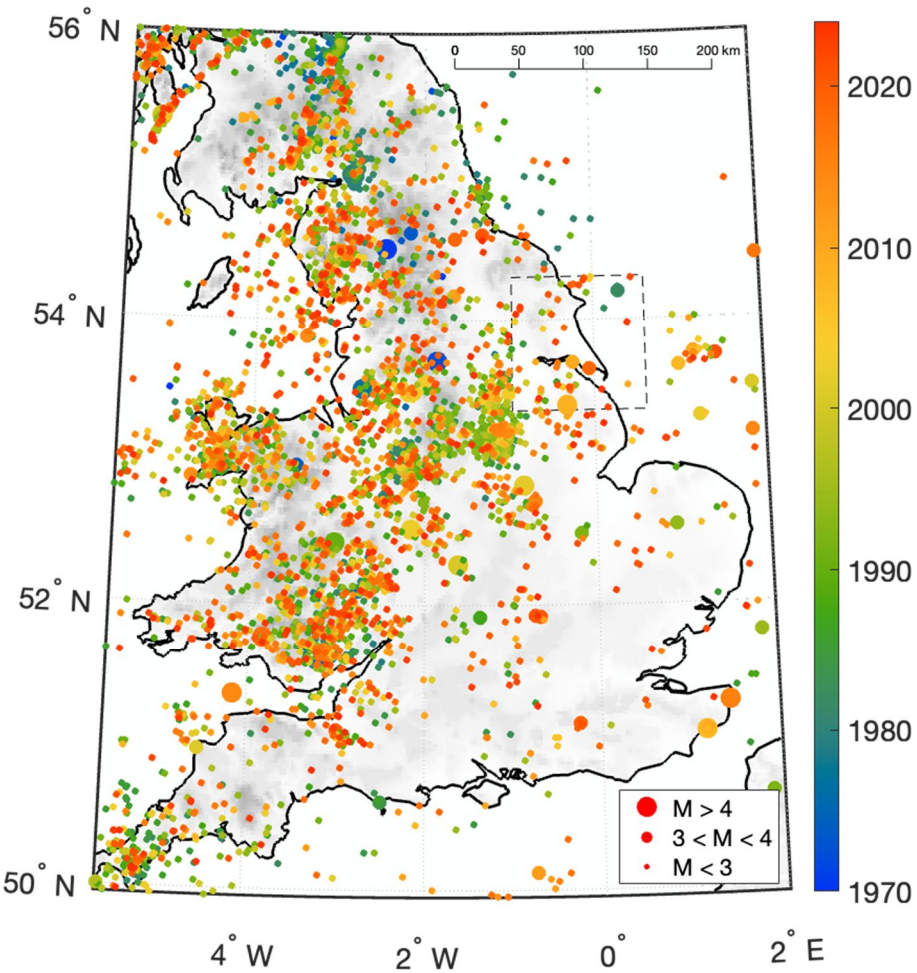

Figure 3.1: Map of earthquakes in England and Wales. Events are coloured by date and sized by magnitude. Rates of seismicity generally decrease from the NW to the SE. The region for this study is shown by the black dashed box.

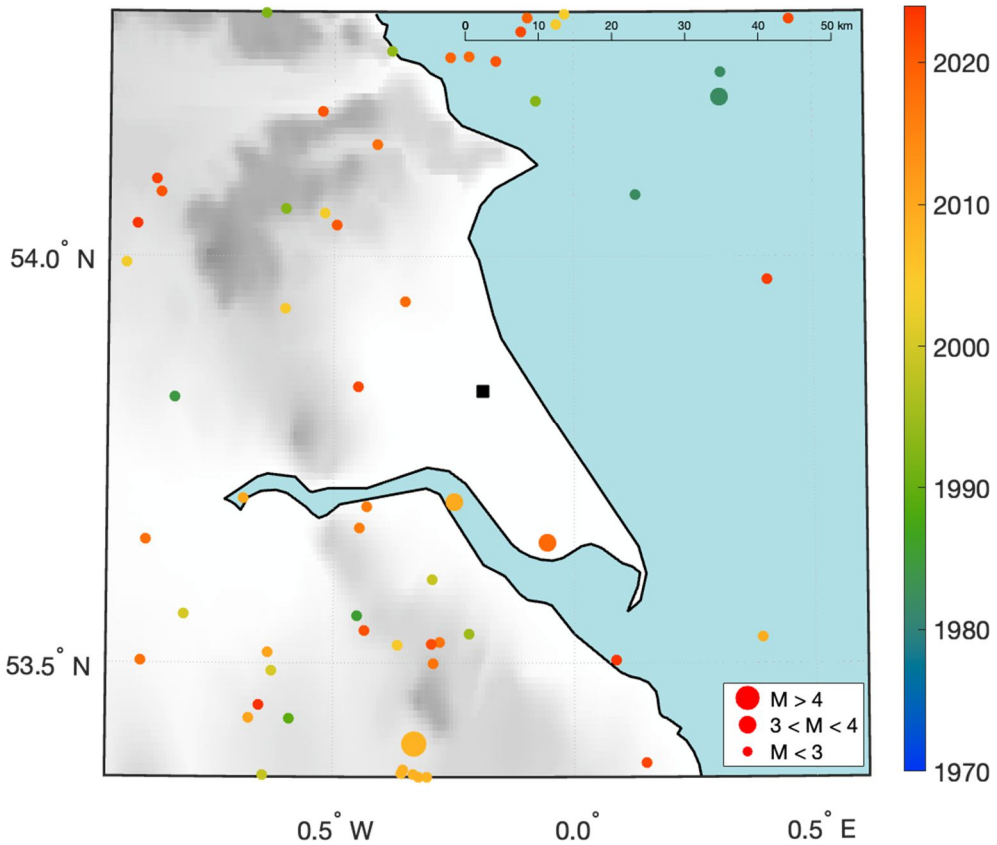

Figure 3.2: Locations of instrumentally recorded earthquakes in a 100 × 100 km region around the West Newton site (black square). Events are coloured by date and sized by magnitude.

The most notable event of interest in the study region is the 2008 M 5.2 Market Rasen earthquake and its associated aftershocks. This event is located roughly 50 km to the south of the West Newton site. The 2008 Market Rasen earthquake was one of the largest earthquakes to have been instrumentally recorded in the UK. It was widely felt across England and Wales. Heyburn and Fox (2010) constrained the depth of this event to 22 km using a combination of surface and body wave observations. At least 12 aftershocks from this event were also detected. This event is accepted to be a tectonic earthquake.

Coal mining has long been associated with induced seismic activity in the UK (e.g., Redmayne, 1988). Indeed, Wilson et al. (2015) estimated that between 20 and 30 % of all earthquakes recorded in the United Kingdom between 1970 and 2012 were induced by coal mining. Magnitudes associated with this activity have been below M 3.0 (Green et al., 2012). However, the areas in which mining-induced seismicity has occurred lie further to the west of our study area.

Figure 3.3 shows the event magnitudes as a function of depth within our study area. Larger events tend to occur at mid-crustal depths, with no events larger than M 3.0 within 10 km depth. Figure 3.4 shows the magnitude-frequency distribution for events within the study area. From this, we estimate a magnitude of completeness (the magnitude above which we can be sure that all events will be detected) of approximately M 2.0. This is consistent with the BGS estimates for detection threshold by the UK's national seismic monitoring system in the area (Galloway, 2022).

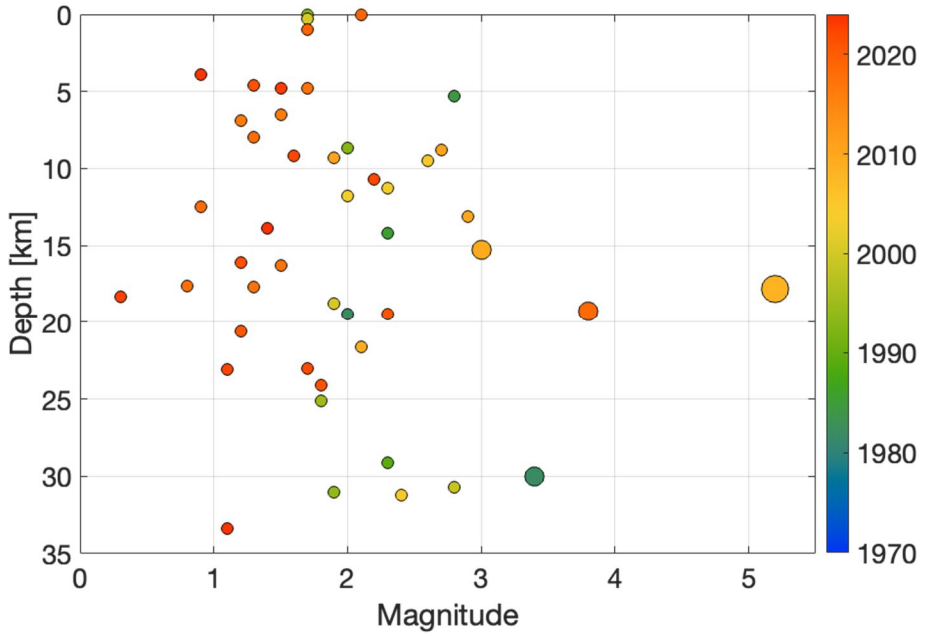

Figure 3.3: Earthquake magnitudes as a function of depth within the study region. Larger earthquakes such as the M_L 5.2 Market Rasen earthquake are found at mid-crustal depths > 10 km. No events larger than M 3.0 are found within 10 km depth.

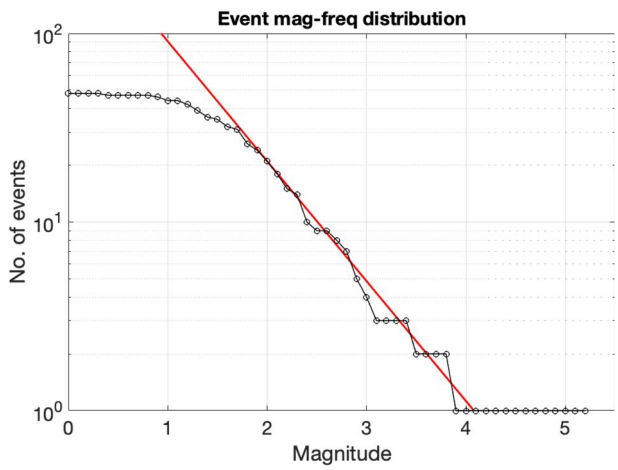

Figure 3.4: Magnitude-frequency distribution (black dots) for the earthquakes shown in Figure 3.2. The events follow a GR distribution with b ≈ 1 (red line), although the 2008 M 5.2 Market Rasen earthquake lies significantly above this trend. The roll-off at low magnitudes begins to occur at M 2.0, indicating the detection threshold for monitoring in this region.

3.2. Hydraulic Fracturing in the West Newton Study Region

Various forms of reservoir stimulation have been carried out in oilfields in the East Midlands, including hydraulic fracturing, proppant squeezes, and acidization (Mustanen et al., 2017). Most of these activities took place between the 1960s – 1990s. However, a small-scale stimulation was carried out in the Wressle W-1 well, just to the south of the Humber Estuary, in 2021. Data for well stimulations has been provided by the North Sea Transition Authority (NSTA). However, because this sort of activity was considered

routine in the oil industry, prior to the recent uptick in public interest around the growth of the shale gas industry, detailed records of fluid injection rates and volumes are often not available. In total, 14 wells were identified within our study area in which stimulation operations have taken place. From an operational perspective the small-scale stimulations carried out in these wells are a good representation of the activities proposed at the West Newton site.

The stimulated wells are mapped in Figure 3.5. These wells are in the Beckingham, Corringham and Gainsborough field to the south of the study area, and the Malton and Kirby Misperton fields in the Vale of Pickering to the north. The primary targets for the fields to the south are Carboniferous-age Millstone Grit or equivalent formations (Ward and Folorunso, 2020), while the primary target for the Vale of Pickering has been the Permian Kirkham Abbey Formation (Harrison et al., 2020).

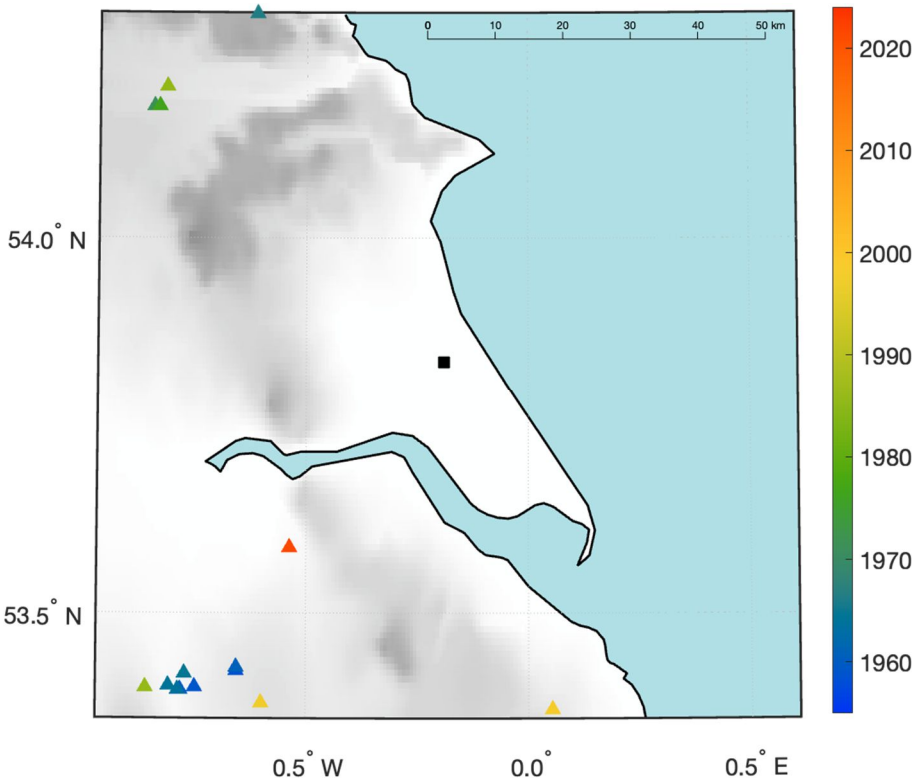

Figure 3.5: Map showing locations of hydraulically stimulated wells in in a 50 km region around the West Newton site (black square). Wells are coloured by stimulation date.

No cases of induced seismicity have been identified or reported from these reservoir stimulation activities. This can be confirmed by comparing stimulated wells with the earthquakes shown in Figure 3.2. In no case is any seismicity found to occur within 5 km and within 30 days of a well stimulation.

The thresholds for event detection, as defined by the magnitude of completeness (the magnitude above which we can be sure that all events will be detected) will have varied during the time period under consideration. Seven of the identified wells were stimulated prior to 1970, the date from which instrumental records for the UK are available. Hence, for wells stimulated prior to 1970 it is reasonable to assume that no earthquakes of sufficient magnitude to be felt at the surface by nearby populations, which

is likely to be between M 2.0 – M 3.0, have occurred. For the 7 wells stimulated during the period for which we have instrumental catalogues, the detection threshold is approximately M 2.0 (Figure 3.4).

At the Wressle W-1 well, which was stimulated in 2021, a dedicated microseismic monitoring array was installed. The detection threshold for this monitoring array was approximately M -1.0. No induced events were detected during the simulation activities, even at very low magnitudes.

The detection thresholds for monitoring arrays during historic stimulation activities poses a limit on definitive conclusions that can be made. It is definitive that no induced events larger than M 3.0 occurred during stimulation of wells prior to the availability of the UK instrumental catalog (1970), no induced events larger than M 2.0 occurred during stimulation of wells after this time, and no induced events larger than M -1.0 occurred during stimulation of the Wressle W-1 well in 2021. These conclusions describe the most conservative case possible based on the detection threshold. Based on our experiences of similar types and scales of activity elsewhere, it is extremely unlikely that any induced seismicity has been associated with the stimulated wells shown in Figure 3.5, except operationally-induced microseismicity that is common to all such activities (with magnitudes typically in the range $-3.0 < M < -1.0$ (Maxwell et al., 2010).

These observations will be taken forward to inform the probabilistic seismic hazard assessment presented in Chapter 6.

4. Geomechanical Appraisal of Fault Stability

In this chapter we perform a geomechanical evaluation of the *in situ* stress conditions and the orientations of mapped faults in order to assess whether the planned stimulation activities are likely to intersect critically-stressed faults. Induced seismicity and fault reactivation seismicity can be understood in terms of the stress conditions relative to the Mohr Coulomb failure threshold (Equation 2.1). It is therefore possible to resolve the *in situ* stress conditions onto mapped faults, and assess whether they are likely to slip. We do so by computing the critical pore pressure, P_C, which represents the increase in pore pressure required for a fault to reach the Mohr-Coulomb failure threshold (assuming the fault has zero cohesion):

$$P_C = \sigma'_n - |\tau|/\mu \tag{4.1}$$

A P_C value of 0 implies that a fault is at the point of criticality, and therefore slip may occur with minimal perturbation. It should be noted that a low P_C value is a necessary but not a sufficient condition for induced seismicity to occur: a fault must also have suitable frictional properties such that the slip occurs rapidly as a seismic event, rather than slow, aseismic slip, and the fault must be close enough to the well that any perturbation is able to reach it. Large P_C values imply that significant pore pressure increases are required to cause slip, and therefore the fault is not critically stressed and is unlikely to produce induced seismicity.

Before beginning this analysis, we note that Rodriguez-Pradilla and Verdon (2024) performed a systematic appraisal of the density of critically-stressed faults across the midlands, finding a general trend that fault densities decreased by an order of magnitude from western England (where induced seismicity has occurred to date) to the east.

Rathlin have mapped potential faults in 3D reflection seismic data at the West Newton site, in which several faults have been identified. These faults form the basis of our fault stability analysis. In general, the Permian section in this area generates relatively smooth structural maps, with no evidence for large faults cross-cutting through the Permian section into over- or underlying strata. There is potentially some evidence for minor intra-Permian faults that are most likely related to early Permian salt dissolution. Rathlin have used various attributes, including coherence and curvature, to map potential small-scale faults through the horizons of interest (Figure 4.1). Here we focus on faults mapped at the Basal Fordon Anhydrite horizon, which is the closest mapped horizon to the target Kirkham Abbey Fomation. Caution should be used when interpreting these features because some could in fact represent changes in depositional facies rather than tectonic structures. Nevertheless, out of an abundance of caution we treat them all as potential fault structures here.

Table 4.1 shows the stress conditions used in our analysis. The stress gradients are derived from proppant squeeze operations at the Wressle W-1 well, roughly 35 km to the south of West Newton, on the southern side of the Humber. These measurements are consistent with regional stress data for the area (Kingdon et al., 2016; Fellgett et al., 2018). The pore pressure gradient was taken from well tests at the adjacent West Newton A-1 well. Based on these gradients, we compute the *in situ* effective stress conditions at the planned depth of operation of the WNA-2 well, 1,750 m TVD.

We begin our analysis by examining the *in situ* stress state for faults of arbitrary orientations. Figure 4.2 shows P_C for all possible fault orientations. The minimum P_C value is -0.7 MPa, implying that an optimally orientated fault could be close to its critical stress. However, this condition can be contrasted with the

stress conditions measured in the Bowland Shale by Clarke et al. (2019), where the minimum P_C value for a fault of arbitrary orientation was as low as -4.4 MPa (Kettlety et al., 2021), implying that faults at that site were much closer to failure at that site.

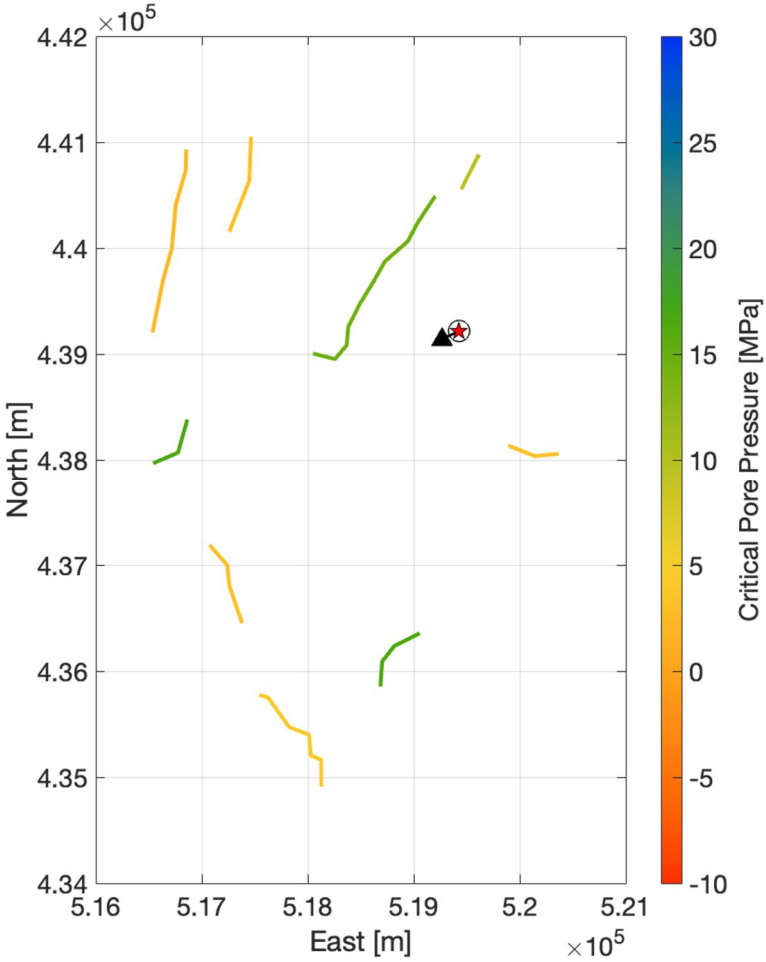

Figure 4.1: Map of faults identified in 3D seismic surveys, coloured by their most likely critical pore pressure value (in MPa). The position of the WNA-2 well is marked by a black triangle, and the planned stimulation point by a red star. The black circle around this point represents a distance of 100 m, which is more than 6 times the planned stimulated fracture length.

Parameter	*Value*	*Uncertainty (1 sd)*
θ_{SH}	*147.5°*	*± 7.4°*
$\Delta\sigma_{Hmax}$	*32 kPa/m*	*± 2 kPa/m*
$\Delta\sigma_{hmin}$	*18.6 kPa/m*	*± 1 kPa/m*
$\Delta\sigma_V$	*24.2 kPa/m*	*± 0.5 kPa/m*
ΔP	*12.7 kPa/m*	*± 0.5 kPa/m*

Table 4.1: Stress orientations and gradients for the WNA-2 geomechanical model.

Each of the parameters in Equation 4.1 is subject to uncertainty, including the in situ stress and pore pressure gradients, the maximum horizontal stress azimuth, the orientation of the faults (from which σ'_n and τ are resolved from the stress tensor), and the friction coefficient μ. Walsh and Zoback (2016) showed how these uncertainties can be incorporated into a fault stability assessment using a Monte Carlo style approach, drawing parameters from within appropriate statistical distributions to create an ensemble of models, from which a probabilistic characterisation of fault stability can be drawn. We follow this approach to assess the stability of the faults identified in Figure 4.1.

We assume that uncertainties for all parameters are normally distributed, with standard deviations given in Table 4.1 for the stress gradients and orientation, and standard deviations of ± 10° for fault strike and dip, and ± 0.1 for μ. For each fault we perform 10,000 model iterations in order to establish a distribution of P_C values for each fault. Figure 4.3 shows the resulting P_C curves, showing the probability that a given increase in pore pressure will exceed the Mohr Coulomb threshold on a given fault. We find that, even for faults that are closest to the optimal orientation, the mean expected P_C value is > 3 MPa, implying a significant perturbation required to enable slip. The likelihood of P_C being ≤ 0 is approximately 30 % or lower for the faults with the lowest P_C values. Again, this can be contrasted with the situation in the Bowland Shale at Preston New Road, where the fault that generated the M 2.9 event in August 2019 had an expected P_C value of -2 MPa, with a 54% likelihood of $P_C \leq 0$ (Kettlety et al., 2021).

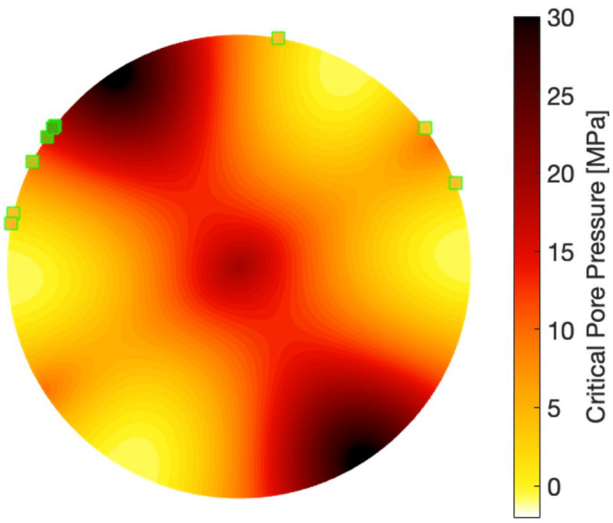

Figure 4.2: Stereographic projection of critical pore pressures at the target depth (see Kettlety et al. 2019, Figure 13 for further explanation). The position within the "ball" represents the fault-normal azimuth and inclination, so the centre of the plot represents a horizontal fault (fault normal vector is vertical), while the edges of the ball represent vertical faults, with a fault running E-W plotting at the top of the ball (fault normal vector azimuth is N-S) and a fault running N-S plotting at the right or left hand edges (fault normal vector azimuth is E-W). P_C values are given in MPa. Green-edged dots show the orientations of faults shown in Figure 4.1.

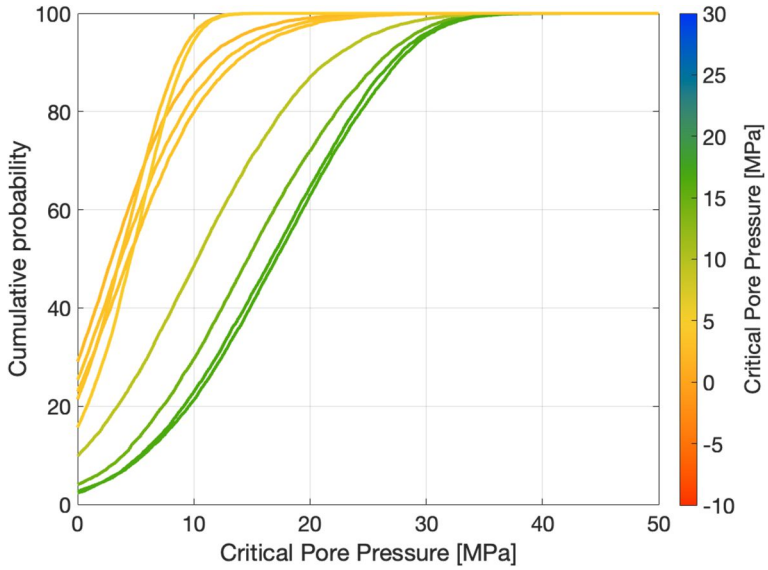

Figure 4.3: Critical pore pressure probability curves for all the faults identified in Figure 4.1. The x-axis shows the critical pore pressure, while the y-axis shows the probability that this pore pressure increase will be sufficient to exceed the Mohr-Coulomb envelop for the fault in question. Curves are coloured by the expected (50%) P_C value.

Figure 4.1 shows the positions of the identified faults relative to the WNA-2 well position. Given the small injection volumes, any perturbations are unlikely to extend any significant distance beyond the injection interval. The small circle around the stimulation point in Figure 4.1 represents a distance of 100 m, which is more than 6 times the planned stimulation distance (16 m). The nearest fault is approximately 1 km from the WNA-2 well, and this fault is not well orientated in the stress field, such that it has a very low likelihood of reactivation (P_C > 10 MPa). The nearest fault that is well-orientated in the stress field is the smaller structure to the southeast, at a distance of roughly 1.2 km.

Hence, we conclude that there are no identified critically-stressed faults within a distance of the WNA-2 well that could be influenced by fluid injection of the scale and volume under consideration in this case. However, despite the absence of mapped faults close to the WNA-2 well, we must also consider the possibility of seismicity occurring on faults that are below the scale of seismic resolution. In the following chapter, we do this by performing a probabilistic seismic hazard assessment.

5. Tolerable Magnitudes

In this chapter we examine the impacts that would be felt by nearby populations if induced events of different magnitudes were to occur. These impacts can be used to establish "tolerable" magnitude thresholds, i.e., the magnitudes that the operator should aim to avoid in order to ensure that intolerable impacts are not felt. Having defined a tolerable magnitude, we can consider what mitigation steps, such as a Traffic Light Scheme or predictive forecasting models (e.g., Verdon and Budge, 2018), could be applied to ensure that M_{TOL} is not exceeded. Importantly, we note that M_{TOL} should not be used to define a red-light traffic light threshold – any such threshold should be set lower than M_{TOL} to enable mitigating actions to be taken before the occurrence of an intolerable magnitude event.

5.1. Method

To estimate the tolerable magnitudes (M_{TOL}) hereafter, we follow the approach of Schultz et al. (2023), whose method was developed specifically for the UK hydraulic fracturing context. In defining M_{TOL}, we do not consider the impacts of magnitude jumps or trailing events (Verdon and Bommer, 2021b). Our approach is demonstrated in Figure 5-1.

The core of the Schultz et al. (2023) method is the estimation of ground motions from an earthquake of a given magnitude. For this we use the ground motion prediction equation (GMPE) of Edwards et al. (2021), which has been developed specifically for hydraulic fracturing-induced earthquakes in the UK. We assume a constant depth of 1.7 km for the induced earthquakes, and locate the event at the position of the West Newton well site. Following Schultz et al. (2023), we model site amplification using a slope-based proxy for V_{S30} (Heath et al., 2020), corrected with non-linear NGA-West2 adjustments to the GMPE (Boore et al., 2014). We incorporate a spatially-correlated intra-event error in ground motions (Esposito and Iervolino, 2012; Edwards et al., 2021). We compute Peak Ground Velocities as the key ground motion metric for nuisance and damage. In our Monte-Carlo sampling (see below), the inputs are each perturbed based on their standard errors.

We translate estimates of PGV across the study area into metrics of nuisance and damage following the criteria of Schultz et al. (2023). PGV-based North American nuisance functions (Schultz et al., 2021) are used to estimate the probability of a given population experiencing nuisance, which is categorized by Community Decimal Intensity (CDI, Wald et al., 2012) with levels ranging from 2-6 corresponding to subjective criteria of 'just felt', 'exciting', 'somewhat frightening', 'frightening', and 'extremely frightening', respectively. Fragility functions based on experience of induced seismicity at the Groningen gas field in the Netherlands (Korswagen et al., 2019) are used to estimate the probability of experiencing damage. We divide damage into two states, with DS1 corresponding to visible light damage (e.g., > 0.1 mm crack) and DS2 corresponding to easily observable light damage (> 1 mm crack). The parameters that define our nuisance and damage functions are perturbed during our Monte Carlo analysis.

The resulting risk is then estimated by considering the numbers of people or households that will experience the defined nuisance or damage. We use a grid of 0.05° × 0.05° (lat/lon) (c. 3.3 × 5.5 km) across which we aggregate UK population data from the LandScan model (Rose et al., 2019).

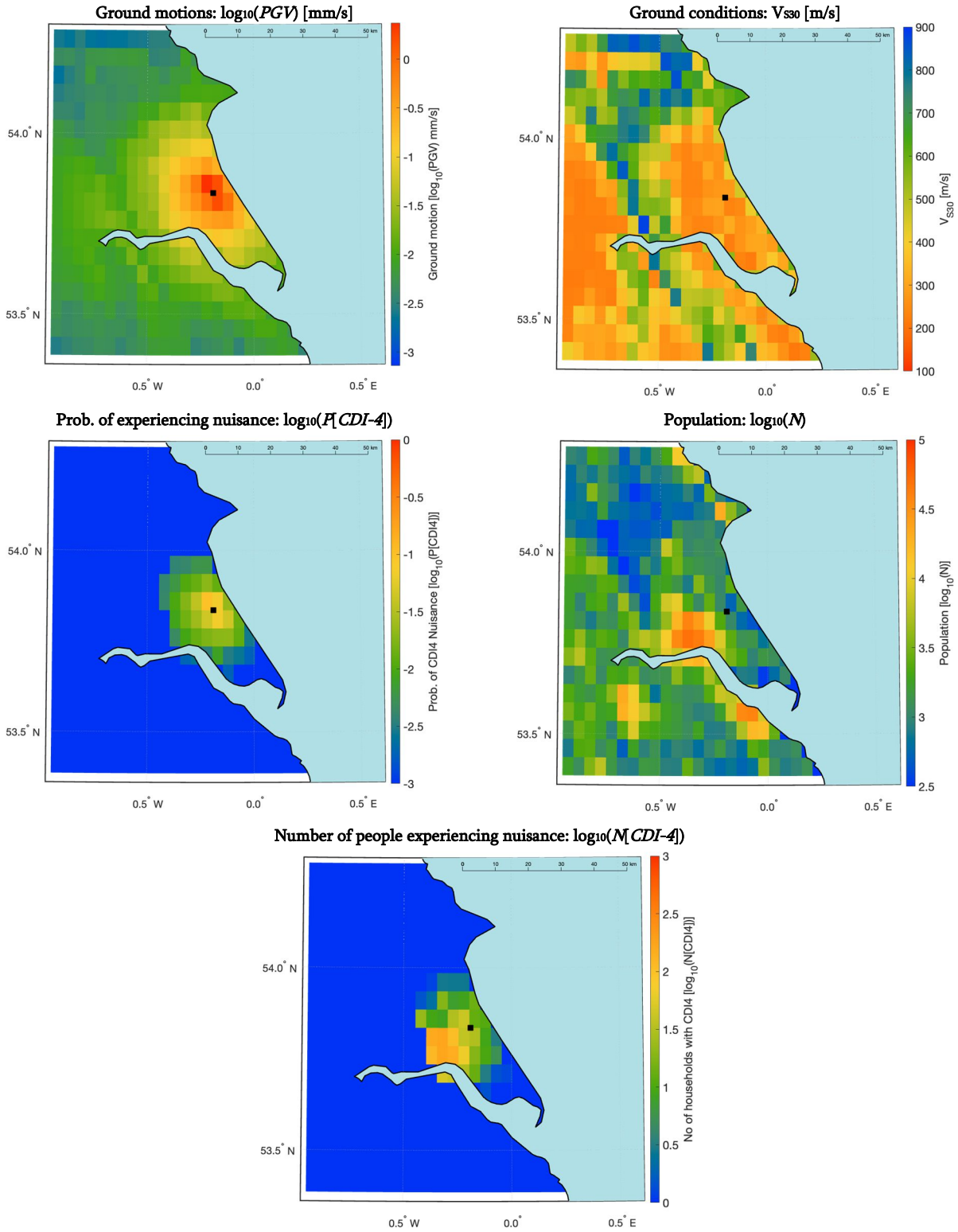

Figure 5-1: Methodology used to estimate tolerable magnitudes, M_{TOL}, for induced seismicity at the West Newton site. We show the PGV generated for an M 3.0 event at the West Newton wellsite. These motions are estimated based on the V_{S30} conditions across the region. Based on these ground motions, we estimate the probability of

experiencing a given nuisance or damage level. These probabilities are multiplied by the numbers of people at each point to estimate the numbers of households that experience the given nuisance/damage.

Given the uncertainties that apply to each of the parameters, we perform a Monte Carlo analysis to capture the range in outcomes produced by the calculations. For a given magnitude event, we perform 3,000 iterations, selecting each parameter that defines the ground motion and the resulting impacts from a distribution based on the standard errors of each parameter. The full distribution of potential outcomes from a given scenario can then be explored.

In order to define whether a given range of impacts is tolerable, we adopt the thresholds developed by Schultz et al. (2023). In defining these thresholds, Schultz et al. (2023) modelled the impacts that occurred for past induced seismicity events in the UK, and whether those impacts could be considered acceptable. For example, after the M 1.6 event during hydraulic fracturing of the Preston New Road PNR-1z well in 2018, the UK government allowed further stimulation activities to take place at the site. In contrast, after the M 2.9 Preston New Road earthquake in 2019, the UK government placed a moratorium on all further hydraulic fracturing at the site. Clearly, therefore, the different levels of impact after these two different events represent qualitative bounds of acceptability in terms of induced seismicity outcomes. This approach produced values of nuisance tolerance (the number of households experiencing the specified level of nuisance) for each CDI level (CDI2 – CDI4) of: T_{CDI2} = 9,571, T_{CDI3} = 5,478, and T_{CDI4} = 2,719. The damage tolerances for DS levels DS1 and DS2 were $T_{DS1} = 10^{-1}$ and $T_{DS2} = 10^{-4}$. The values of T_{DS1} and T_{DS2} being less than 1 imply a probability of 1-in-10 that a single home experiences damage at level DS1, and a probability of 1-in-10,000 that a single home experiences damage at level DS2. Schultz et al. (2023) define the tolerable magnitude as the magnitude at which the median estimated impacts exceed these thresholds.

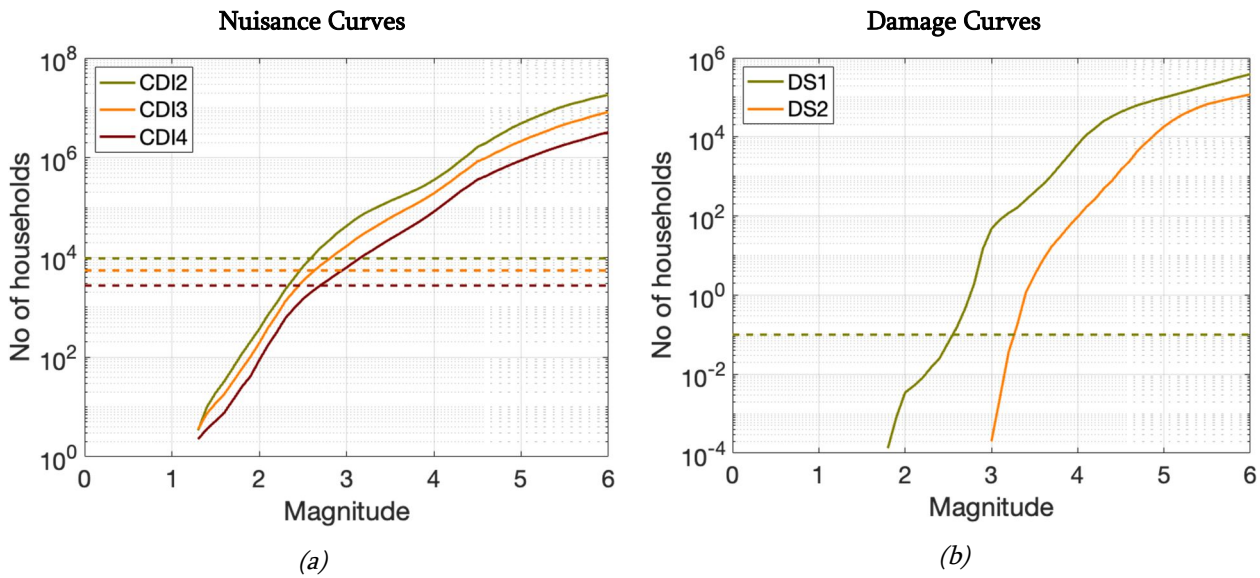

Figure 5-2: Nuisance (a) and damage (b) curves for an earthquake at the West Newton wellsite, showing the numbers of households that would experience different impact criteria for a given magnitude event. The dashed lines show the tolerable thresholds for different impacts as defined by Schultz et al. (2023).

5.2. Results

The median seismic impact curves are shown in Figure 5-2. These curves show the numbers of households experiencing a given nuisance or damage level as a function of magnitude for an earthquake located at the West Newton site. The tolerable thresholds as defined by Schultz et al. (2023) are also shown. We find that each of the tolerable criteria are reached at magnitudes between $2.5 \leq M_{TOL} \leq 3.0$. We therefore adopt a tolerable threshold for induced seismicity at the West Newton site of $M_{TOL} = 2.5$. Induced earthquake with magnitudes larger than this may produce impacts that might not be tolerable for the local population. Having established this threshold, we can then consider whether the proposed operations are likely to generate induced seismic events of this magnitude, and therefore whether any mitigative strategies are required during operations.

6. Seismic Hazard Assessment

In this Chapter we perform a seismic hazard assessment for the stimulation activities proposed for the WNA-2 well. The objective of the seismic hazard assessment process is to estimate the likelihood that induced seismicity magnitudes reach a given threshold. We apply a probabilistic approach, based on well-established links between injection volumes and induced seismicity rates, calibrated using observations of HF-IS around the world, to compute the expected largest event magnitudes for the proposed operation. The likelihood of induced events of a given magnitude can be compared with the M_{TOL} estimates made in the previous chapter in order to ascertain whether any additional induced seismicity hazard mitigation might be required.

6.1. Maximum Magnitudes

The establishment of constraints on the magnitude of the largest earthquake, M_{MAX}, that is considered to be physically possible, given the tectonic settings in question, can be an important element of induced seismicity hazard assessment. We note that this value describes the largest event that could possibly occur, not the largest event that is likely to occur – the M_{MAX} magnitude will likely have a very low probability of occurrence. The question of an appropriate M_{MAX} for hydraulic stimulation in the UK remains relatively unconstrained. It is almost certainly less than the tectonic values for the UK of M 6.5 used by Mancini et al. (2021), but it is probably larger than the M 3.0 estimated by Green et al. (2012), given that magnitudes reached M 2.9 during hydraulic fracturing at Preston New Road (Bommer and Verdon, 2024).

The role of M_{MAX} in seismic hazard assessment is to remove the contribution of unfeasibly large magnitudes that would otherwise be generated by an unbounded extrapolation of the GR distribution. Hence, its significance will depend on whether events of that size are in play given the estimated recurrence parameters. If events of a size within a range of possible M_{MAX} choices are considered very unlikely to occur based on the expected recurrence, then the choice of M_{MAX} value becomes relatively unimportant. This was in fact the case for the Mancini et al. (2021) Preston New Road study – while they chose an M_{MAX} of M 6.5, the likelihood of events larger than M 3.0 generated by their model-based forecasting was very small, and so their choice for the M_{MAX} parameter was immaterial.

In our analysis we do not attempt to estimate an M_{MAX} value, instead leaving the upper tail of the Gutenberg-Richter distribution unbounded, since the likelihoods of reaching magnitudes that could be relevant to this consideration are so low as to be immaterial (see below).

6.2. Event Recurrence Rate Estimates

We can use the concept of the seismogenic index Σ, described in Chapter 2, to estimate the likelihood of events exceeding a given magnitude based on an unbounded Gutenberg-Richter distribution with a given recurrence rate. Equation 2.4 shows that the seismogenic index, combined with the injected volume V, describes the total number of events that will occur that are larger than magnitude M (Shapiro et al., 2010). If the occurrence of individual events within the overall GR distribution can be treated as an independent Poissonian process, then the probability that an event larger than M does not occur if a total volume V_T is injected can be calculated as:

$$\mathbb{P} = \exp\left(-V_T \times 10^{\Sigma - bM}\right). \tag{6.1}$$

We can rearrange this equation to arrive at a forecast for the largest event that will occur during operations, which we refer to here as M_{MAX}^{M} (noting that this is different from the largest event that could possibly occur based on tectonic and geomechanical considerations, M_{MAX}, as described in the previous section). For a given confidence level χ, the event magnitude that will not be exceeded is given by:

$$M_{MAX}^{M} = \frac{\left(\Sigma - \log\left[\frac{-\ln(\chi)}{V_T}\right]\right)}{b}. \tag{6.2}$$

If Σ is known then we can use this equation to forecast the largest expected event size. Figure 6.1 shows an example calculation of M_{MAX}^{M} likelihood for a given combination of b, V_T and Σ. This approach has been successfully applied for real-time forecasting of seismicity that occurred at the Preston New Road wells (Clarke et al., 2019). This approach was also used to manage induced seismicity during stimulation of a geothermal energy plant in Helsinki (Kwiatek et al., 2019), and to forecast induced seismicity due to wastewater disposal in Oklahoma (e.g., Langenbruch and Zoback, 2016).

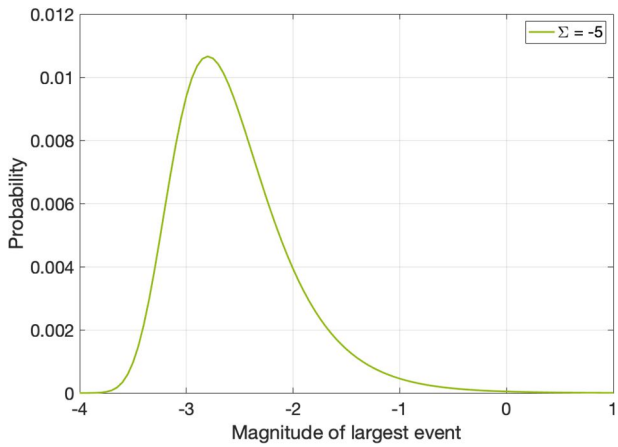

Figure 6.1: Example of the largest expected event magnitude, M_{MAX}^{M}, based on a given injection volume and seismogenic index. The green curves shows the likelihood of M_{MAX}^{M} with Σ = -5, b = 1, and an injection volume of V_T = 150 m³.

However, whereas during operations Σ can be determined by comparing the rate of seismicity with the injected volume, for an a priori study of HF-IS, potential values of Σ must be inferred, based on observations of HF-IS elsewhere. The appropriate framework within which to consider this source of uncertainty is with a logic tree. In seismic hazard assessment, a logic tree describes potential choices for a parameter, with each branch carrying a weight that reflects the likelihood of that choice being the most appropriate.

There are a number of factors that influence the logic tree for Σ that we adopt for the West Newton site. In general, the abundance of faulting in this area is low, and there are no recorded instances of HF-IS, despite numerous reservoir stimulation operations taking place in the region. The Kirhkam Abbey Formation is found within the Permian section, with evaporite layers found both above and below. As discussed in Chapter 2, the presence of evaporites can serve as a geomechanical and hydraulic barrier to stress and pressure transfers into surrounding strata, significantly limiting the ability of such formations to generate induced seismicity. The Kirkham Abbey formation is over-pressured, which can be a risk

factor for HF-IS. However, from our geomechanical analysis, there are no mapped critically-stressed faults in the vicinity of the WNA-2 well.

Looking across global datasets, values for Σ observed by Dinske and Shapiro (2013) for hydraulic fracturing range between -9 to -4. Values for Σ observed by Verdon and Budge (2018), Schultz et al. (2018), and Clarke et al. (2019) for hydraulic fracturing in some of the more seismogenic shale plays such as the Horn River and Duvernay Shales in the WCSB, and the Bowland Shale at Preston New Road, range from $-2.5 \geq \Sigma \geq -0.5$. However, the is no reason to expect elevated values for Σ at West Newton, given the nature of the operation and the regional context.

Perhaps the best constraint for Σ comes from the Wressle W-1 well, which is just to the south of the Humber Estuary, a distance of approximately 35 km. Reservoir stimulation at this well was conducted in 2021, and a dedicated surface monitoring array was installed. No induced events were detected during this operation, with a detection threshold of approximately M -1.0. The injection volume at Wressle W-1 was 150 m^3. We can use Equation 6.2 to constrain an upper bound for Σ at the Wressle site. Assuming 1 event could have occurred with a magnitude just below the detection threshold, Equation 6.2 yields an upper bound for Σ of -3.3. There are some differences between the Wressle and West Newton sites, most notably the target formation. As above, the presence of evaporites above and below the Kirkham Abbey Formation may render this formation less seismogenic.

Following Rodriguez-Pradilla and Verdon (2024), we adopt a normal distribution for Σ, with a mean value of -4.0 and a standard deviation of 1 unit. This distribution is shown in Figure 6.2. The upper tail allows for Σ values as high as -1.0 (albeit at low probabilities), which is towards the upper levels observed at Preston New Road, while the lower tail extends to values as low as -7.0, which is towards the globally observed lowermost values for hydraulic fracturing compiled by Dinske and Shapiro (2013). This distribution is consistent with the (lack of) seismicity observed at the Wressle W-1 well.

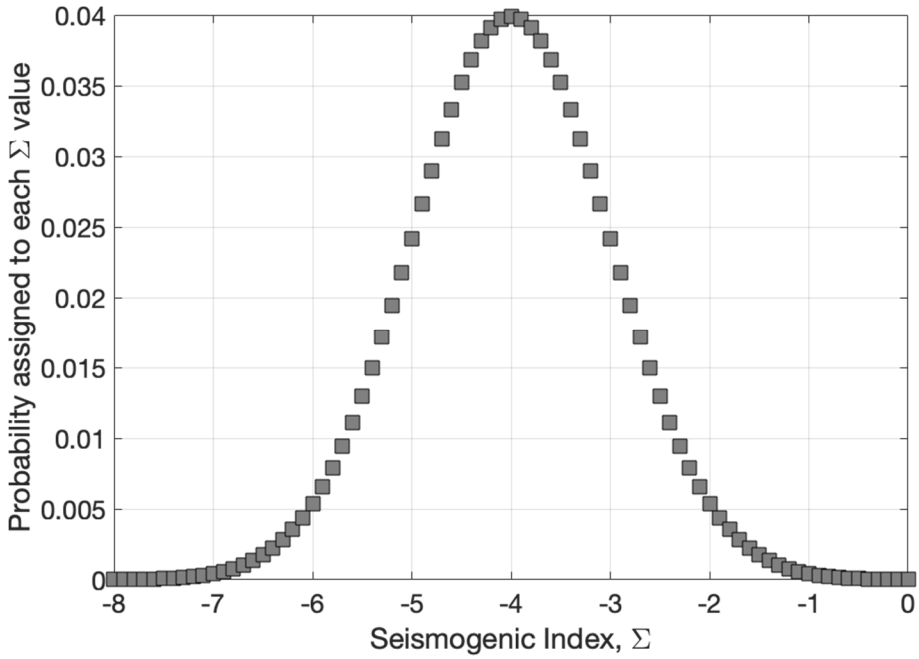

Figure 6.2: Probabilities assigned to Σ values in our logic tree. Our distribution is centred on Σ = -4.0, with a standard deviation of 1 unit.

6.3. Probabilistic Seismic Hazard Estimates

We use Equation 6.2 to compute the likelihoods for a given largest magnitude M_{MAX}^{M} event, weighting each individual Σ value by its likelihood as shown in Figure 6.2, and summing over all possible Σ values. We assume a *b* value of 1.0, and an injection volume of 62 m³, which is the planned injection volume for the WNA-2 well. The results are plotted in Figure 6.3.

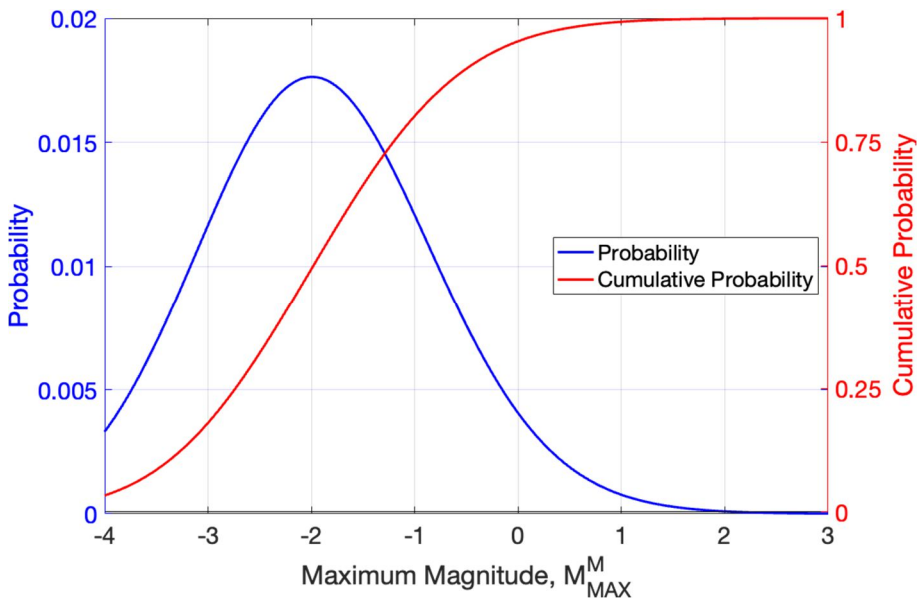

Figure 6.3: Probability and cumulative probability for the largest event size, M_{MAX}^{M}, produced by combining each of the Σ scenarios shown in Figure 6.2.

We find that the most likely largest event size from the proposed operation is a magnitude of M -2.0. There is a 95 % likelihood that the largest event size is less than M 0.0, and the extreme case, with a 1% chance of exceedance, is a largest event with magnitude M 0.8. Since these values fall well below the range of potential values for the largest tectonically possible event, M_{MAX}, constraining this value is not necessary for the purposes of our assessment.

In Chapter 5, we established the maximum tolerable magnitude, at which point the impacts of induced seismicity could become unacceptable to local communities, finding that M_{TOL} = 2.5 for the West Newton site. Our estimated likelihood of reaching or exceeding this threshold is 0.024 % (roughly 1-in-4,000).

Based on our impact modelling (Chapter 5), our 1 % event (the magnitude that has a 1 % chance of being reached or exceeded) of M 0.8 will not be felt by any households.

The most likely M_{MAX}^{M} value is a magnitude of M -2.0. An event of this size would be too small to be detected using a local array of surface seismometers, and may even be at the limit of what can be detected using a downhole geophone array, depending on its noise levels and configuration. In other words, the

most likely scenario is that the largest event during the proposed operation is too small to be detected even using a downhole array.

6.4. Comparison with Recent Hydraulic Fracturing in the UK

We can make comparisons between these model results and observations during recent instances of hydraulic fracturing in the UK. On the Fylde Peninsula, hydraulic fracturing in the Bowland Shale has generated several cases of induced seismicity. As described above, fault densities in western England are higher, and the stress conditions in the Bowland Shale are closer to criticality, meaning that higher seismogenic index values are expected.

Nevertheless, after the first stage of stimulation of the Preese Hall well in 2011, in which over 1,800 m^3 of fluid was injected, no seismicity was observed. Although monitoring at this site was only provided by the national seismic network at the time, use of a matched-filter event detection approach allowed the detection of events down to M 0.0 (Clarke et al., 2014). Hence, we can conclude that at Preese Hall, the injection of 1.5 orders of magnitude (i.e., 30 times) more fluid than proposed for WNA-2, into a more seismogenic formation, did not produce any events larger than M 0.0.

For the Preston New Road PNR-1 well, downhole microseismic data is publicly available, along with detailed injection data. This shows that, after injection of 100 m^3, all of the observed microseismicity was below M -1.5 (when converted into the UK's local magnitude scale). For the PNR-2 well, which ultimately generated an M 2.9 event, the first stage injected roughly five times the volume of fluid as that intended for the proposed WNA-2 operation. However, the only event detected by the surface monitoring array had a magnitude of M -0.2. Again, these operations show that similar (or larger) injection operations, into a formation that is known to be relatively seismogenic, did not generate seismicity of sufficient magnitude to be felt at the surface, and indeed the magnitudes of any microseismic events that were generated were significantly below this threshold. Larger seismic events only occurred at these wells after injection of significantly larger volumes.

At the Wressle W-1 well, roughly 2.5 times the injection volume planned for WNA-2 was used. The Wressle site is approximately 35 km from West Newton, although it targeted a deeper, and therefore potentially more seismogenic formation. Nevertheless, no induced seismicity was detected during that operation, despite the installation of a dedicated local seismicity monitoring array that had a potential detection threshold as low as M -1.0.

7. Conclusions

The operators of the West Newton field plan to conduct a reservoir stimulation operation in the WNA-2 well. In such an operation, fluid is injected to create a small fracture network that is filled with proppant, providing a permeable connection with the reservoir. While the term "hydraulic fracturing" can be used as a catch-all term for such operations, the key factor here is the scale: whereas hydraulic fracturing in shale gas reservoirs, which has generated concern over the potential for induced seismicity, uses 1000s of m^3, injected via multiple stages along horizontal wells, proppant squeeze operations typically use less than 200 m^3, with a single injection stage. Given the induced seismicity is observed to scale with the volume of fluid injected, the hazard posed by the proposed reservoir stimulation is significantly lower than that of large scale shale gas stimulation.

The region has experienced extensive use of reservoir stimulation techniques, from the late 1950s until the 2000s. In total, 14 such wells have been identified within 100 × 100 km of the West Newton site. There is no recorded seismicity associated with any of these activities, indicating that the hazard posed by such operations is low.

We have performed a geomechanical assessment of faults around the WNA-2 well identified using 3D seismic survey data. The nearest fault is over 1 km from the well, far further than the maximum expected fracture length of 16 m. The state of stress on the faults is moderate – the smallest mean expected perturbation required to reactivate any of the identified faults is 3 MPa: a perturbation of this magnitude at a distance of over 1 km, given the proposed operation, is very unlikely. However, studies of observed faults cannot rule out the potential for undetected faults on which seismicity could occur. Hence, we perform a probabilistic assessment of seismic hazard for the proposed operation.

To estimate the recurrence rate, we make use of the scaling between injection volume and earthquake rate that is widely established for injection-induced seismicity. When combined with the GR distribution, this allows us to make a forecast of the largest expected event magnitude. The scaling coefficient between volume and rate – the seismogenic index – is poorly constrained, so we use a logic tree that extends across the range of observed values, with strongest weighting at mid-range values. This logic tree includes values for seismogenic index that are towards the top end of those observed in the most seismogenic shale plays.

The resulting assessment produces a most likely largest event magnitude of M -2.0. An event of this size would not be detectable at the surface, and might be at the limit of detectability for a downhole system. Our assessment indicates a 95% probability that events do not exceed M 0.0, a level that could be detected by a local seismic monitoring array, but would not be felt by the nearby public. Our extreme case, with a 99% probability that it is not exceeded, is a maximum magnitude of M 0.8. Such an event would not be felt by the public nearby.

As such, we conclude that the proposed activities pose a very low risk with respect to seismic hazard. The likelihood of reaching magnitudes that could be tolerable to the local public is negligible. We do not believe that the installation of local seismicity monitoring arrays is warranted, given (a) the very low levels of risk posed by the proposed operation, and (b) the high likelihood that magnitudes will not reach the threshold of detectability for the array, meaning that no microseismicity would be detected. Furthermore, the planned injection volume is so low that the injection process itself will be very short. This would leave

no window for reactive decision-making in response to recorded induced seismicity, rendering any monitoring data of very little operational use.

References

AER, 2019a. Subsurface Order No. 6, Alberta Energy Regulator. Available at: https://static.aer.ca/prd/documents/orders/subsurface-orders/SO6.pdf.

AER, 2019b. Subsurface Order No. 7. Alberta Energy Regulator. Available at: https://static.aer.ca/prd/documents/orders/subsurface-orders/SO7.pdf.

Babaie Mahani, A., R. Schultz, H. Kao, D. Walker, J. Johnson, C. Salas, 2017. Fluid injection and seismic activity in the Northern Montney Play, British Columbia, Canada, with special reference to the 17 August 2015 M_W 4.6 induced earthquake: Bulletin of the Seismological Society of America 107, 542-552.

Babaie Mahani, A., H. Kao, G.M. Atkinson, K. Assatourians, K. Addo, Y. Liu, 2019. Ground-motion characteristics of the 30 November 2018 injection-induced earthquake sequence in northeast British Columbia, Canada: Seismological Research Letters 90, 1457-1467.

BCOGC, 2012. Investigation of observed seismicity in the Horn River Basin. B.C. Oil and Gas Commission: Available online at https://www.bcogc.ca/node/8046/download.

Clarke, H., L. Eisner, P. Styles, P. Turner, 2014. Felt seismicity associated with shale gas hydraulic fracturing: the first documented example in Europe: Geophysical Research Letters 41, 8308-8314.

Clarke, H., J.P. Verdon, T. Kettlety, A.F. Baird, J-M. Kendall, 2019. Real time imaging, forecasting and management of human-induced seismicity at Preston New Road, Lancashire, England: Seismological Research Letters 90, 1902-1915.

Deng, K., Y. Liu, R.M. Harrington, 2016. Poroelastic stress triggering of the December 2013 Crooked Lake, Alberta, induced seismicity sequence: Geophysical Research Letters 43, 8482-8491.

Dinske, C. and S.A. Shapiro, 2013. Seismotectonic state of reservoirs inferred from magnitude distributions of fluid-induced seismicity: Journal of Seismology 17, 13-25.

Edwards, B., H. Crowley, R. Pinho, J.J. Bommer, 2021. Seismic hazard and risk due to induced earthquakes at a shale gas site: Bulletin of the Seismological Society of America 111, 875-897.

Esposito, S. and I. Iervolino, 2012. Spatial correlation of spectral acceleration in European data: Bulletin of the Seismological Society of America 102, 2781-2788.

Eyre, T.S., D.W. Eaton, D.I. Garagash, M. Zecevic, M. Venieri, R. Weir, D.C. Lawton, 2019. The role of aseismic slip in hydraulic fracturing-induced seismicity: Science Advances 5, eaav7172.

Farahbod, A.M., H. Kao, D.M. Walker, J.F. Cassidy, 2015. Investigation of regional seismicity before and after hydraulic fracturing in the Horn River Basin, northeast British Columbia: Canadian Journal of Earth Sciences 52: 112-122.

Fellgett, M.W., A. Kingdon, J.D.O. Williams, C.M.A. Gent, 2018. Stress magnitudes across UK regions: new analysis and legacy data across potentially prospective unconventional resource areas: Marine and Petroleum Geology 97, 24-31.

Friberg, P.A., G.M. Besana-Ostman, I. Dricker, 2014. Characterization of an earthquake sequence triggered by hydraulic fracturing in Harrison County, Ohio: Seismological Research Letters 85, 1925-1307.

Galloway, D.D., 2022. The British Geological Survey Earthquake Bulletin for 2021. BGS Report OR/22/005.

Green, C. A., P. Styles, B.J. Baptie, 2012. Preese Hall shale gas fracturing review and recommendations for induced seismic mitigation: Department of Energy and Climate Change, London.

Gutenberg, B., and C. F. Richter, 1944. Frequency of earthquakes in California: Bulletin of the Seismological Society of America 34, 185-188.

Hallo, M., I. Oprsal, L. Eisner, M.Y. Ali, 2014. Prediction of magnitude of the largest potentially induced seismic event: Journal of Seismology 18, 421-431.

Harrison, D., M. Haarhoff, M. Heath-Clarke, W. Hodgson, F. Hughes, D. Ware, A. Mortimer, 2020. The Vale of Pickering gas fields: Kirby Misperton, Malton, Mrishes and Pickering, North Yorkshire, UK Onshore: Geological Society of London Memoirs 52, 82-93.

Heath, D.C., D.J. Wald, C.B. Worden, E.M. Thompson, G.M. Smoczyk, 2020. A global hybrid Vs30 map with a topographic slope–based default and regional map insets: Earthquake Spectra 36, 1570-1584.

Heyburn, R. and B. Fox, 2010. Multi-objective analysis of body and surface waves from the Market Rasen (UK) earthquake: Geophysical Journal International 81, 532-544.

Hincks, T., W. Aspinall, R. Cooke, T. Gernon, 2018. Oklahoma's induced seismicity strongly linked to wastewater injection depth: Science 359, 1251-1255.

Hubbert, M.K. and D.G. Willis, 1957. Mechanics of hydraulic fracturing: Transactions of Society of Petroleum Engineers of AIME 210, 153-163.

Kettlety, T., J.P. Verdon, M. Werner, J-M. Kendall, 2020. Stress transfer from opening hydraulic fractures controls the distribution of induced seismicity: Journal of Geophysical Research 125, e2019JB018794.

Kettlety T., J.P. Verdon, A. Butcher, M. Hampson, L. Craddock, 2021. High-resolution imaging of the ML 2.9 August 2019 earthquake in Lancashire, United Kingdom, induced by hydraulic fracturing during Preston New Road PNR-2 operations: Seismological Research Letters 92, 151-169.

Kingdon, A., M.W. Fellgett, J.D.O. Williams, 2016. Use of borehole imaging to improve understanding of the in-situ stress orientation of Central and Northern England and its implications for unconventional hydrocarbon resources: Marine and Petroleum Geology 73, 1-20.

Korswagen, P., M. Longo, E. Meulman, L. Licciardello, M. Sousamli, 2019. Damage sensitivity of Groningen masonry – experimental and computational studies: Part 2, NAM Report by Delft University of Technology.

Kwiatek, G., T. Saamo, T. Ader, F. Bluemle, M. Bohnhoff, M. Chendorain, G. Dresen, P. Heikkinen, I. Kukkonen, P. Leary, M. Leonhardt, P. Malin, P. Martinez-Garzon, K. Passmore, P. Passmore, S. Valenzuela, C. Wollin, 2019. Controlling fluid-induced seismicity during a 6.1-km-deep geothermal stimulation in Finland: Science Advances 5, eaav7224.

Langenbruch, C. and M.D. Zoback, 2016. How will induced seismicity in Oklahoma respond to decreased saltwater injection rates? Science Advances 2, e1601542.

Lei, X., D. Huang, J. Su, G. Jiang, X. Wang, H. Wang, X. Guo, H. Fu, 2017. Fault reactivation and earthquakes with magnitudes up to M_W 4.7 induced by shale-gas hydraulic fracturing in Sichuan Basin, China: Scientific Reports 7, 7971.

Lei, X., Z. Wang, J. Su, 2019. The December 2018 M_L 5.7 and January 2019 M_L 5.3 earthquakes in South Sichuan Basin induced by shale gas hydraulic fracturing: Seismological Research Letters 90, 1099-1110.

Mancini, S., M.J. Werner, M. Segou, B. Baptie, 2021. Probabilistic forecasting of hydraulic fracturing-induced seismicity using an injection-rate driven ETAS model: Seismological Research Letters 92, 3471-3481.

Maxwell, S.C., J. Rutledge, R. Jones, M. Fehler, 2010. Petroleum reservoir characterization using downhole microseismic monitoring: Geophysics 75, A129-A137.

Montgomery, C.T. and M.B. Smith, 2010. Hydraulic fracturing history of an enduring technology: Journal of Petroleum Technology 62, 26-41

Mustanen D., J Fianu, J. Pucknell, 2017. Account of hydraulically fractured onshore wells in the UK and seismicity associated with these wells: Journal of Petroleum Science and Engineering 158, 202-221.

NRC, 2013. Induced Seismicity Potential in Energy Technologies: The National Academies Press, Washington, DC.

Pawley, S., R. Schultz, T. Playter, H. Corlett, T. Shipman, S. Lyster, T. Hauck, 2018. The geological susceptibility of induced earthquakes in the Duvernay Play: Geophysical Research Letters 45, 1786-1793.

Redmayne, D.W., 1988. Mining induced seismicity in UK coalfields identified on the BGS national seismograph network, in Engineering Geology of Underground Movements, eds F.G. Bell, M.G. Culshaw, J.C. Cripps, M.A. Lovell, 405–413, Geological Society Engineering Geology Special Publication 5.

Rodriguez-Pradilla, G., and J.P. Verdon, 2024. Quantifying the variability in fault density across the UK Bowland Shale, with implications for induced seismicity hazard: Geomechanics for Energy and the Environment 38, 100534.

Rose, A., J. McKee, M. Urban, E. Bright, K. Sims, 2019. LandScan 2018 high-resolution global population data set: Oak Ridge National Laboratory, Oak Ridge, TN, United States.

Rubinstein, J.L. and A. Babaie Mahani, 2015. Myths and facts on wastewater injection, hydraulic fracturing, enhanced oil recovery, and induced seismicity: Seismological Research Letters 86, 1060-1067.

Schultz, R., R. Wang, Y.J. Gu K. Haug, G. Atkinson, 2017. A seismological overview of the induced earthquakes in the Duvernay play near Fox Creek, Alberta: Journal of Geophysical Research 122, 492-505.

Schultz, R., G. Atkinson, D.W. Eaton, Y.J. Gu, H. Kao, 2018. Hydraulic fracturing volume is associated with induced earthquake productivity in the Duvernay play: Science 359, 304-308.

Schultz, R., V. Quitoriano, D.J. Wald, G.C. Beroza, 2021. Quantifying nuisance ground motion thresholds for induced earthquakes: Earthquake Spectra 37, 789-802.

Schultz, R., B. Baptie, B. Edwards, S. Wiemer, 2023. Red-light thresholds for induced seismicity in the UK: Seismica 2, 1086.

Shapiro, S.A. and C. Dinske, 2009. Fluid-induced seismicity: pressure diffusion and hydraulic fracturing: Geophysical Prospecting 57, 301-310.

Shapiro, S.A., C. Dinske, C. Langenbruch, F. Wenzel, 2010. Seismogenic index and magnitude probability of earthquakes induced during reservoir fluid stimulations: The Leading Edge 29, 304-308.

Skoumal, R.J., M.R. Brudzinski, B.S. Currie, 2015. Earthquakes induced by hydraulic fracturing in Poland Township, Ohio: Bulletin of the Seismological Society of America 105, 189-197.

Skoumal, R.J., M.R. Brudzinski, B.S. Currie, 2018. Proximity of Precambrian basement affects the likelihood of induced seismicity in the Appalachian, Illinois, and Williston basins, central and eastern United States: Geosphere 14, 1365-1379.

Skoumal, R.J., A.J. Barbour, M.R. Brudzinski, T. Langenkamp, J.O. Kaven, 2020. Induced seismicity in the Delaware Basin, Texas: Journal of Geophysical Research 125, e2019JB018558.

Terzaghi, K., 1943. *Theoretical Soil Mechanics,* John Wiley and Sons, New York.

van der Elst, N.J., M.T. Page, D.A. Weiser, T.H.W. Goebel, S.M. Hosseini, 2016. Induced earthquake magnitudes are as large as (statistically) expected: Journal of Geophysical Research Solid Earth 121, 4575-4590.

Verdon, J.P., 2014. Significance for secure CO_2 storage of earthquakes induced by fluid injection: Environmental Research Letters 9, 064022.

Verdon, J.P. and J. Budge, 2018. Examining the capability of statistical models to mitigate induced seismicity during hydraulic fracturing of shale gas reservoirs: Bulletin of the Seismological Society of America 108, 690-701.

Verdon, J.P., and J.J. Bommer, 2021a. Comment on "Activation rate of seismicity for hydraulic fracture wells in the Western Canadian Sedimentary Basin" by Ghofrani and Atkinson (2020): Bulletin of the Seismological Society of America 111, 3459-3474.

Verdon J.P. and J.J. Bommer, 2021b. Green, yellow, red, or out of the blue? An assessment of Traffic Light Schemes to mitigate the impact of hydraulic fracturing-induced seismicity: Journal of Seismology 25, 301-326

Verdon, J.P., and G. Rodriguez-Pradilla, 2023. Assessing the variability in hydraulic fracturing-induced seismicity occurrence between North American shale plays: Tectonophysics 859, 229898.

Vilarrasa, V. and J. Carrera, 2015. Geologic carbon storage is unlikely to trigger large earthquakes and reactivate faults through which CO_2 could leak: Proceedings of the National Academy of Sciences 112, 5938-5943.

Wald, D.J., V. Quitoriano, C.B. Worden, M. Hopper, J.W. Dewey, 2012. USGS "Did You Feel It?" internet-based macroseismic intensity maps: Annals of Geophysics 54, 688-707.

Walsh F.R. and M.D. Zoback, 2016. Probabilistic assessment of potential fault slip related to injection-induced earthquakes: application to north-central Oklahoma, USA: Geology 44, 991-994.

Ward, K.L., and F.O. Folorunso, 2020. The Corringham, Gainsborough-Beckingham, Glentworth, Nettleham, Stainton and Welton fields, UK onshore: Geological Society of London Memoirs 52, 45-54.

Wilson, M.P., R.J. Davies, G.R. Foulger, B.R. Julian, P. Styles, J.G. Gluyas, S. Almond, 2015. Anthropogenic earthquakes in the UK: a national baseline prior to shale exploitation: Marine and Petroleum Geology 68, 1-17.

Yoon, C.E., Y. Huang, W.L. Ellsworth, G.C. Beroza, 2017. Seismicity during the initial stages of the Guy-Greenbrier, Arkansas, earthquake sequence: Journal of Geophysical Research 122, 9253-9274.

OUTER LIMITS